Low Actuation Voltage Capacitive Shunt RF-MEMS Switch Using a Corrugated Bridge with HRS MEMS Package

Yo-Tak Song[1] · Hai-Young Lee[1] · Masayoshi Esashi[2]

Abstract

This paper presents the theory, design, fabrication and characterization of the novel low actuation voltage capacitive shunt RF-MEMS switch using a corrugated membrane with HRS MEMS packaging. Analytical analyses and experimental results have been carried out to derive algebraic expressions for the mechanical actuation mechanics of corrugated membrane for a low residual stress. It is shown that the residual stress of both types of corrugated and flat membranes can be modeled with the help of a mechanics theory. The residual stress in corrugated membranes is calculated using a geometrical model and is confirmed by finite element method(FEM) analysis and experimental results. The corrugated electrostatic actuated bridge is suspended over a concave structure of CPW, with sputtered nickel(Ni) as the structural material for the bridge and gold for CPW line, fabricated on high-resistivity silicon(HRS) substrate. The corrugated switch on concave structure requires lower actuation voltage than the flat switch on planar structure in various thickness bridges. The residual stress is very low by corrugating both ends of the bridge on concave structure. The residual stress of the bridge material and structure is critical to lower the actuation voltage. The Self-alignment HRS MEMS package of the RF-MEMS switch with a 15 Ω · cm lightly-doped Si chip carrier also shows no parasitic leakage resonances and is verified as an effective packaging solution for the low cost and high performance coplanar MMICs.

Key words : Low-Actuation Voltage, RF-MEMS, Capacitive Shunt Switch, Microwave and Millimeter-Wave, Corrugated Bridge, Residual Stress, HRS MEMS Package, Self-Alignment.

Ⅰ. Introduction

Microelectromechanical systems(MEMS) are small mechanical devices fabricated with standard integrated circuit(IC) technology, offering the advantages of mass production with excellent uniformity in device properties over the whole wafers.

In recent years, wireless communication has grown rapidly and has made an explosive growth of the radio frequency(RF), microwave and millimeter-wave applications[1]. In these applications, RF switch is the essential component to operate RF circuit. MEMS electrostatic actuated reflective switches for low-loss microwave and millimeter-wave applications have recently been reported [2]~[4]. RF-MEMS switches offer superior performance such as low insertion loss, high isolation, lower power consumption, excellent signal linearity, better impedance match and less dispersion compared to conventional semiconductor switches based on PIN diodes or GaAs field effect transistors(FETs)[5],[6]. Therefore, such switches are very desirable for applications with demands on high signal integrity, despite their slow switching time.

The first MEMS switch was already shown in 1978 as electrostatic actuated cantilever switch[7], and the first RF-MEMS switch was shown in 1991, consisting of an electrostatic actuated rotating transmission line switch[8]. However, those switches needed high actuation voltages of 80~200 V.

Most of the RF-MEMS switches reported to date have used electrostatic actuation[9]~[12], which normally requires high actuation voltages(20~80 V). Electrostatic actuation offers extremely low power consumption and easy implementation. However, there are two main challenging issues for RF-MEMS switches actuated by electrostatic force: lowering the actuation voltage and increasing mechanical stability. The high actuation voltage requires high voltage drive circuits, degrades life time and induces malfunction by charge trapping problem.

There are many varieties of RF-MEMS switches. The switches can be in series[11] or in shunt[13] with the signal path and coupling can be either metal-to-metal[14] or capacitive[2].

The two basic RF-MEMS switches from a function

Manuscript received April 26, 2006 ; revised June 9, 2006. (ID No. 20060426-011J)

[1]Department of Electronics Engineering, Ajou University, Suwon, Korea.

[2]Department of Nanomechanics, Graduate School of Engineering, Tohoku University, Japan.

perspective are series switch and shunt switch. The former is usually realized as metal-contact switch able to switch signal from DC to radio frequency with high isolation. Most of the shunt switches are based on variable capacitance short-circuiting the signal line in the down-state. The isolation of such capacitive shunt switches is very low for lower frequency due to its capacitive short-circuiting principle but their performance is much better at higher frequency in the millimeter-wave. Furthermore, such switches are usually smaller, easier to fabricate, show higher reliability comparing susceptible metal contacts in stiction and degradation, and have been investigated more thoroughly than the series switches[10]. Typical applications for the different types of switches are e.g. in the fields of microwave radar and telecommunication systems for capacitive shunt switches, and automated test equipment(ATE) for series shunt switches. However, metal-contact series switches have also been used successfully in the microwave frequency, as in delay networks up to 40 GHz[15].

The main disadvantage of those switches is high actuation voltage. Recently, those types of the switches have been improved[16]~[18] and the other types of the switches have implemented. The actuation mechanisms of other types are based on electromagnetic[19],[20] and thermal[21] principles. The switches based on electromagnetic actuation have low actuation voltage but consume high power and have complex fabrication process. On the other hand, thermal actuated switches have high power consumption. If the actuation voltage of the electrostatic switches is low, then the electrostatic switches will be the best candidate in RF mobile system applications.

Most of RF MEMS switches utilize rotator[22], cantilever[4], and membrane structure[2],[3] for electrostatic actuators. Various designs of capacitive RF-MEMS switches made of electroplated nickel[9], aluminum[2] and gold[23] have been so far reported in literatures.

In recent years, much effort has been put on to decrease the actuation voltage of the electrostatic switches. Those efforts include using a variety of beam geometries and materials to decrease the spring constant of the beam, increase the area of the electrostatic field, decrease the gap and increase the dielectric constant between two plates of the switch. Variations in those parameters cause a loss on the other parameters of the switches[24].

In this paper, the proposed structure for decreasing in actuation voltage is based on decreasing in effective spring constant from the effective Young's modulus by corrugated membrane. Analytical analysis studies of membranes with corrugations have been so far reported in literatures of microphones[25]~[28]. As mentioned here, an expression for the residual stress of corrugated membranes with intrinsic residual stress is deduced from an algebraic description of geometrical modeling. There, the reduction of the effective residual stress is estimated by measuring and comparing the electrostatic actuation voltage of a corrugated and flat membrane. The effective residual stress reduction due to stretching of the corrugations is derived analytically and confirmed by experimental results. Analytical analyses are proved by experimental results on the effective residual stress of corrugated membranes. The static deflection and the stress of the bridges are also obtained by the finite element method(FEM) analysis. Finally, the application of such membranes in RF-MEMS switch is demonstrated. A very good agreement between theory and experimental results is demonstrated for corrugated and flat switches of various thickness membranes.

We describe the experimental results of a low actuation voltage capacitive shunt RF-MEMS switch based on a corrugated electrostatic actuated bridge suspended over a concave structure of coplanar waveguide(CPW), with sputtered nickel as the structural material for the bridge and gold for CPW line, fabricated on high-resistivity silicon(HRS) substrate using IC compatible processes for modular integration in a communication devices.

The corrugated bridge of the concave structure requires a lower actuation voltage 20~80 V compared to a 50~100 V of the flat bridge of the planar structure in a 0.3 to 1.0 μm thick Ni capacitive shunt RF-MEMS switch. The effective residual stresses in 0.3 to 1.0 μm thick Ni membranes for the RF-MEMS switches are measured and calculated about 3~15 MPa in the corrugated structure and 30 MPa in the flat structure. The intrinsic residual stress is about 30 MPa regardless of the various thickness membranes in the flat bridge. The residual stress is very low by corrugating both ends of the bridge on concave structure. The residual stress of the bridge material and structure is critical to lower the actuation voltage.

The self-alignment packaged switch has two states: when the bridge is up, the signal passes through with less than 1.0 dB insertion loss, 15 dB return loss and 10 dB power loss up to 40 GHz. When the bridge is down, the signal is attenuated by 28 dB isolation and power loss 10 dB up to 40 GHz.

II. Design

2-1 Corrugated Membrane Mechanics

In order to actuate the switch, the center conductor of the CPW line is biased with respect to the ground by

DC voltage. The resulting electrostatic force pulls the bridge toward the center conductor, with a pull-down voltage of

$$V_P = V(2g_0/3) = \sqrt{\frac{8k}{27\varepsilon_0 Ww}\, g_0^3} \tag{1}$$

where k is the effective spring constant of the bridge, W is the CPW center conductor width, w is the bridge width, ε_0 is the permittivity of free space, and g_0 is the nominal gap height.

Equation 1 leads to some obvious ideas for reducing the pull-down voltage. The actuation voltage can be lowered by reducing the spring constant, reducing the gap, or increasing the electrode areas. Reducing the spring constant is one with the most flexibility.

The spring constant k consists of k' due to the stiffness of the membrane which accounts for the material characteristics such as Young's modulus E and k'' due to the biaxial residual stress σ within the beam and the fabrication process, therefore the spring constant k is found by adding k' and k''.

The general expression of those spring constants k' and k'' for a concentrated load at the center of the beam is

$$k' = 32Ew\left(\frac{t}{l}\right)^3 \frac{1}{8(x/l)^3 - 20(x/l)^2 + 14(x/l) - 1} \tag{2}$$

$$k'' = 8\sigma(1-v)w\left(\frac{t}{l}\right)\frac{1}{3-2(x/l)}\,. \tag{3}$$

For a beam over a CPW line with the center conductor width being a third of the length of the beam with a force distributed above the center conductor, the spring constant k of the bridge added k' and k'' with $x=2l/3$ results in

$$k(x=2l/3) = 32Ew\left(\frac{t}{l}\right)^3\left(\frac{27}{49}\right) + 8\sigma(1-v)w\left(\frac{t}{l}\right)\left(\frac{3}{5}\right) \tag{4}$$

where E is the Young's modulus of the bridge material, v is the Poisson's ratio, σ is the tensile residual stress, w is the bridge width, t is the bridge thickness, and l is the bridge length, as shown in Fig. 1[29]~[32].

The thinner the thickness of the bridge is, the more the residual stress in the spring constant is dominant in Eq. 4. The spring constant is thought to be related to residual stress in the bridge, since the bridge deflection in response to an applied actuation voltage becomes dominated by the residual stress even with the existence of minute stress level. Consequently, releasing the residual stress in the bridge is a key for a low actuation voltage. Corrugation can strongly decrease the effective residual stress of the bridge with high intrinsic tensile residual stress. Thus, we have implemented the idea of using a corrugated bridge to release the spring constant in the switch.

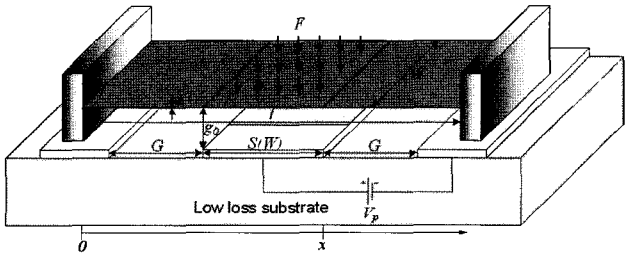

Fig. 1. Bridge with the distributed electrostatic force about the center.

The tensile residual stress in a corrugated membrane is significantly reduced by an elongation of the corrugation structures. For relatively high stresses and/or shallow corrugations, the increased bending stiffness in a tangential direction can be neglected, and a corrugated membrane with intrinsic residual stress σ_0 acts like a flat membrane with corrugated residual stress σ in equilibrium.

For this purpose, the effective residual stress is calculated using a geometric model of a corrugation structure shown in Fig. 2. One half of the corrugation structure consists of the cantilevers with lengths $d/2$, $b/2$, and height h. The height of the corrugation h should be much smaller than the length d, therefore the deflection of the short cantilever is negligible. For a lateral force F, the bending angle θ of the long cantilever with length $d/2$ and moment of inertia $I=w\cdot t^3/12$ are calculated using the moment $M_{max}=F\cdot h\cos\theta$

$$\theta(rad) = \int \frac{M(x)}{E\cdot I}\,dx = \frac{1}{E\cdot I}\cdot\frac{M_{\max}}{l}\int_0^l x\cdot dx \tag{5}$$

$$\theta = \frac{1}{E\cdot I}\int_0^{d/2} M(x)\cdot dx = \frac{6\cdot\cos\theta\cdot F\cdot\left(\frac{d}{2}\right)\cdot h}{E\cdot w\cdot t^3} \tag{6}$$

where E denotes the Young's modulus, w the width of the cantilever, t its thickness, and l cantilever length, respectively.

Thus, the displacement $\triangle x$ for one corrugation and small angle is given by

$$\triangle x = 2\cdot\sin\theta\cdot h \approx 2\cdot\theta\cdot h = \frac{6\cdot\cos\theta\cdot F\cdot d\cdot h^2}{E\cdot w\cdot t^3} \tag{7}$$

For $h/t \gg 1$, when there is a lateral residual stress σ_0, the corresponding lateral displacement $\triangle x$ is mainly due to the bending of the corrugation wall, and is approximately calculated with the following Eq. 8. If $F=\sigma_0 wt$,

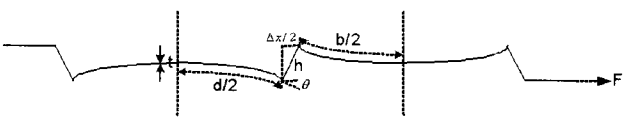

Fig. 2. Model of a corrugation loaded by a lateral force.

$$\triangle x=\frac{6\cdot\sigma_0\cdot\cos\theta\cdot d}{E}\cdot\left(\frac{h}{t}\right)^2. \quad (8)$$

If the elastic displacement of a cantilever is $\triangle x=F\cdot d/E\cdot w\cdot t$ and $\cos\theta\approx1$ in small angle θ, the effective Young's modulus E_{eff} is then defined as follows.

$$E_{eff}=\frac{F\cdot d}{\triangle x\cdot w\cdot t}=\frac{E\cdot t^2}{6\cos\theta\cdot h^2}\approx\frac{1}{6}\cdot E\cdot\left(\frac{t}{h}\right)^2 \quad (9)$$

Hence, a corrugated membrane can be considered to behave as if it is a flat membrane with an effective Young's modulus E_{eff} defined above, as far as the lateral displacement perpendicular to the corrugation wall is concerned. A model of a corrugated membrane with a number of corrugations $N\cdot(d+b)$ and a flat membrane of length a is depicted in Fig. 3.

Under thermal stress, the sum of elastic(suffix e) and thermal(suffix t) displacements of the corrugated(index c) and flat(index f) region must be zero.

$$\triangle x_c^e+\triangle x_c^t+\triangle x_f^e+\triangle x_f^t=0 \quad (10)$$

Using the elastic and the thermal displacements of N corrugated region $\triangle x_c^e=F\cdot N\cdot(d+b)/(w\cdot t\cdot E_{eff})$ and $\triangle x_c^t$, $=\alpha\cdot\triangle T\cdot(\alpha_0\cdot\triangle T\cdot N\cdot(d+b))$ the elastic and the thermal displacements of a flat region $\triangle x_f^e=F\cdot a/(w\cdot t\cdot E)$ and $\triangle x_f^t=\alpha_0\cdot\triangle T\cdot a$, where α and α_0 are called the thermal expansion coefficients of corrugated and flat region, and $\triangle T$ is the change in temperature, Equation 10 is rewritten as

$$\frac{F\cdot N\cdot(d+b)}{E_{eff}\cdot w\cdot t}+\frac{F\cdot a}{E\cdot w\cdot t}+$$
$$\alpha\cdot\triangle T\cdot(\alpha_0\cdot\triangle T\cdot N\cdot(d+b))+\alpha_0\cdot\triangle T\cdot a=0. \quad (11)$$

Thus, the effective residual stress $\sigma=-F/w\cdot t$ in a whole corrugated membrane as a function of the thermal stress $\sigma=\alpha\cdot\triangle T\cdot E_{eff}$ and $\sigma_0=\alpha_0\cdot\triangle T\cdot E$ of corrugated and flat membrane is given by

$$\sigma=\frac{E_{eff}\cdot\sigma_0\cdot a}{E\cdot N\cdot(d+b)+E_{eff}\cdot a-\sigma_0\cdot N\cdot(d+b)} \quad (12)$$

The corrugation releases the intrinsic residual stress σ_0, and the effective residual stress in the whole membrane due to the corrugations becomes

$$\sigma=\frac{E_{eff}\sigma_0 l_2}{El_1+E_{eff}l_2-\sigma_0 l_1} \quad (13)$$

where l_1 and l_2 are the lengths of corrugated and flat region, respectively.

Since usually $E\gg\sigma_0$, the effective residual stress strongly depends on the corrugation length, depth and the membrane thickness

$$\sigma\approx\frac{E_{eff}\cdot\sigma_0\cdot a}{E\cdot N\cdot(d+b)+E_{eff}\cdot a}\approx\frac{\sigma_0}{1+\frac{6\cdot N\cdot(d+b)}{a}\cdot\left(\frac{h}{t}\right)^2} \quad (14)$$

where the length of the membrane is $l=2a+2N\cdot(d+b)$. The most important parameters are the corrugation height h, length $N\cdot(d+b)$ and membrane thickness t. For a large ratio h/t, the effective residual stress is proportional to $(t/h)^2$ and decreases almost linearly with the length of corrugations $N\cdot(d+b)$[25]~[28].

2-2 Capacitive Shunt RF-MEMS Switch Design

A capacitive shunt RF-MEMS switch consists of a thin metal membrane, called the bridge, which can be electrostatically actuated to the transmission line using a DC bias voltage, suspended over a dielectric layer deposited on top of the center conductor and fixed at both ends to the ground conductors of a coplanar waveguide (CPW) line. A dielectric layer is used for DC isolation of the bridge from the CPW center conductor. When an electrostatic potential is applied between the center conductor and the ground, the attractive electrostatic force pulls the bridge down towards the dielectric layer. The dielectric layer serves to prevent electrical contact and stiction between the center conductor and the bridge, and yet provides a low impedance path between the two contacts. Once the bias voltage is released, the mechanical stress in the bridge overcomes the attractive force and pulls up the bridge away from the dielectric layer, returning it to the original position. When the bridge is up, the switch presents a small shunt capacitance to ground. When the bridge is pulled down to the center conductor, the shunt capacitance increases by a factor of C_d/C_u=20~100 presenting a RF short-circuit, as shown in Fig. 4[32].

The single capacitive shunt switch is modeled using both series sections of transmission-line and a lumped CLR(capacitor-inductor-resistor) model of the bridge with

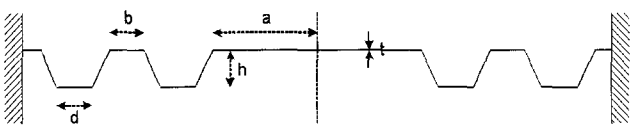

Fig. 3. Model of a corrugated membrane.

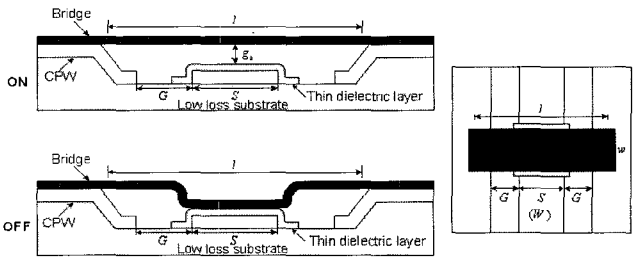

Fig. 4. ON/OFF model of the capacitive shunt switch.

the capacitance having an up-state and a down-state position. The impedance of the shunt switch is given by

$$Z_s = 1/j\omega C + j\omega L + R_s \quad \text{with} \quad C = C_u \text{ or } C_d \tag{15}$$

depending on the position of the bridge, as shown in Fig. 5. The LC series resonant frequency and the impedance of the shunt switch can be approximated by

$$Z_s = \begin{cases} 1/j\omega C & f \ll f_0 \\ R_s & \text{for } f = f_0 \text{ of } f_0 = \dfrac{1}{2\pi\sqrt{LC}} \\ j\omega L & f \gg f_0 \end{cases} \tag{16}$$

Also, a further consideration in the design for low actuation voltage is that lowering the actuation voltage is made up of the corrugated membranes at the both ends of the bridge. The bridges are created on a concave structure for the corrugated bridge compared to a planar structure for the flat bridge in order to measure the intrinsic residual stress.

The single capacitive shunt RF-MEMS switch is designed on a CPW line with dimensions of G/S/G=65/100/65 μm(50 Ω impedance matching) on a high-resistivity silicon(HRS: ε_r=11.9, 10 kΩ · cm) substrate for 0.5~40 GHz frequencies. The membrane material of the switch is the sputtered Ni (E=200 GPa, ν=0.31) for high Young's Modulus and thin membrane. The membrane length l of the switch is 300 μm, the CPW center conductor width l is 100 μm, the membrane width w is 100 μm, the membrane gap height g_0 is 4 μm, and the membrane thickness t is 0.3~1.0 μm by 0.1 μm step for the comparison of the residual stress. The length of the flat region is a=147.5 μm at the center of the bridge. The length and the height of the corrugated region are $N \cdot (d+b)$=1 · 2.5 μm and h=3 μm at the both ends of the bridge, respectively. Therefore, the residual stress ratios σ / σ_0 of the bridges with corrugated structure are 0.09~0.52 due to the various thickness

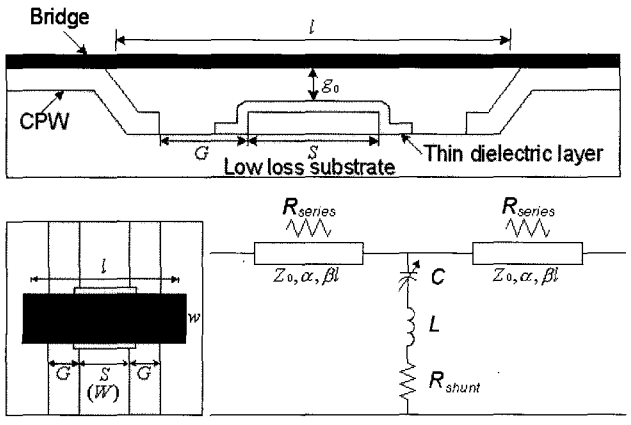

Fig. 5. Circuit model of the capacitive shunt switch.

membrane t 0.3~1.0 μm by 0.1 μm step.

The HRS MEMS package is also designed using p-type HRS (10 kΩ · cm) 〈100〉 wafers as cover layer. The cover layer using HRS can be defined by standard Si MEMS process based on a controlled wet-etching technique in which the etching rate is determined by the TMAH etchant. In order to match the 50 Ω characteristic impedance on feed-through lines, the package needs the alignment of the cover layer width with the tapered feed-through length[33],[34].

Ⅲ. Fabrication

The RF-MEMS switch is implemented on a 525 μm-thick 〈100〉 high-resistivity silicon(HRS) wafer with resistivity of 10 kΩ · cm. Initially a 0.75 μm thermal oxide layer is grown on the wafer, followed the bulk wet etching by TMAH(Tetra Methyl Ammonium Hydroxide, $(CH_3)_4NOH$, etch rate 0.5 μm/min by thermal oxide masking at 80 ℃) for CPW reference plane with 5 μm-depth concave structure. The CPW line is defined using a photolithography process by evaporating a layer of Au (1 μm) with Ti adhesion layer (200 Å). Next, a 1,500 Å PECVD(Plasma-Enhanced Chemical Vapor Deposition) silicon nitride (Si_3N_4) or TEOS(Tetra Ethyl Ortho Silicate) oxide layer is deposited and patterned to form the dielectric layer between the bridge and the signal line. A 4 μm-thick sacrificial layer of photoresist is then coated and patterned. The thickness of this layer determines the nominal gap height g_0 of the bridge. And then, the membrane has been uniformly sputtered with Ni (0.3~1.0 μm with 0.1 μm step) by DC faced target sputter and finally patterned. To avoid collapsing the membrane during drying, the bridge is released using a critical point drying system.

To avoid the bridge crack and peeling during sputtering, the temperature and the time of the hardbake before sputtering are 145 ℃ and 1 hour in convection oven, respectively. And, to make the low tensile stress in the sputtered Ni, the vacuum pressure of the sputter is increased from 10 mTorr to 5 mTorr. The process flow charts are shown in Fig. 6 for the corrugated switch with package on concave structure and the flat switch with package on planar structure.

The structure after patterning of the sacrificial layer is a key design parameter determining the corrugated structure. The mask design is an important role in fabricating the corrugated structure. And, the actuation voltage can be lowered by the decrease of the corrugation ratio, which is achieved by the decrease of the membrane thickness at the same corrugation length and height conditions as shown in Eq. 14.

The RF-MEMS switches are fabricated using the corru-

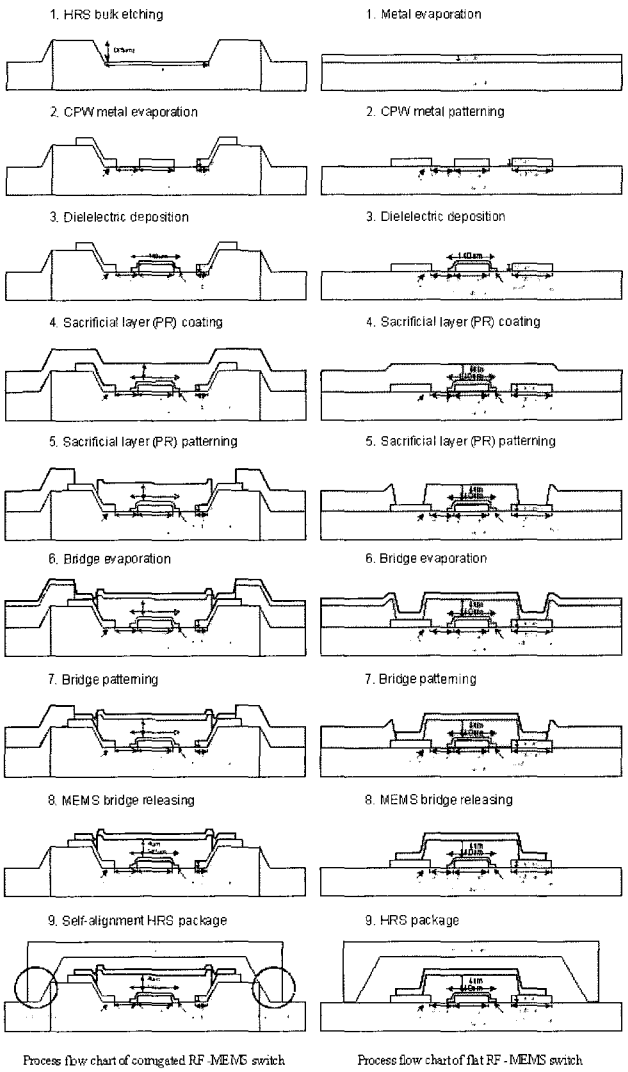

Fig. 6. Process flow charts of the RF-MEMS switch.

gated membrane on the concave structure and the flat membrane on the planar structure as shown in Fig. 7.

The cover layer width for the 50 Ω characteristic impedance matching of the tapered feed-through length on the RF-MEMS switch is determined by considering the inclination (54.7°) effects of the HRS wafer using the thermal oxide (SiO_2 7500 Å) and the TMAH anisotropic silicon bulk etchant. For the proposed package, the 10 μm-depth cavity for the HRS cover layer is then fabricated with a 525 μm-thick HRS substrate by photolithography and dicing process, and placed on the RF-MEMS switch using a nonconductive epoxy, as shown in Fig. 8[33],[34].

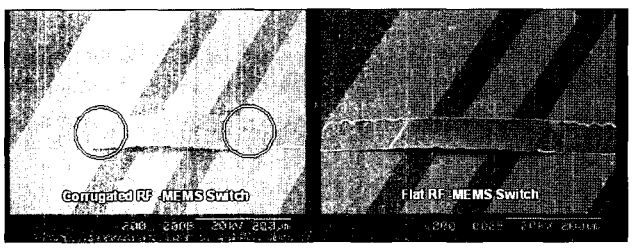

Fig. 7. SEM photograph of the fabricated RF-MEMS switch.

In order to self-align the cover with the RF-MEMS switch, both layers are fabricated by tapered structure. The capacitive shunt RF-MEMS switch and HRS package are fabricated for self-alignment package on the tapered CPW by an elevated place as shown in Fig. 9. The full package is self-aligned on the tapered CPW by an elevated place as shown in Fig. 10.

The capacitive shunt RF-MEMS switch with HRS MEMS package having a corrugated membrane in the concave structure is shown in Fig. 11.

Ⅳ. Measurements

4-1 Finite Element Simulation

In order to predict the mechanical properties of the bridge, the deflection and the stress of the bridge are calculated by finite element method(FEM) analysis tool (ANSYS 8.1) with real values. In modeling the bridges, Shell element (SHELL63) in ANSYS is used to describe the flat and corrugated structures. The elastic Young's modulus and Poisson's ratio of nickel are 200 GPa and

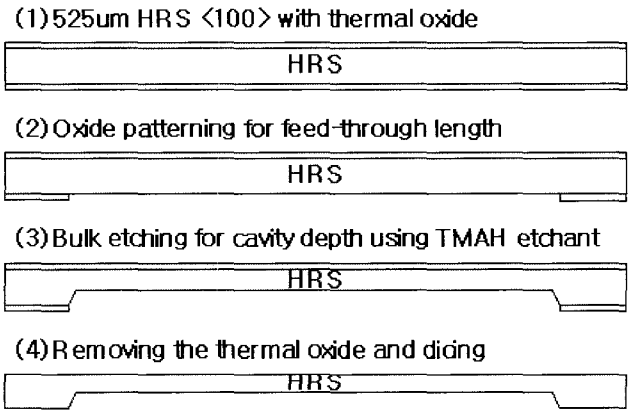

Fig. 8. Process flow chart for the cover layer.

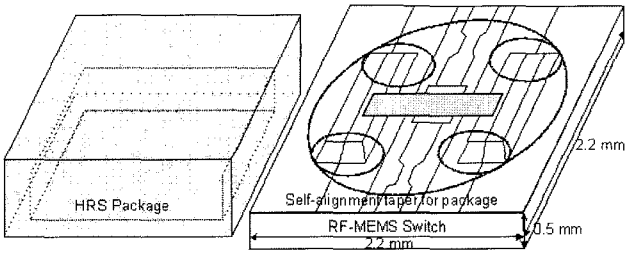

Fig. 9. RF-MEMS switch and HRS package.

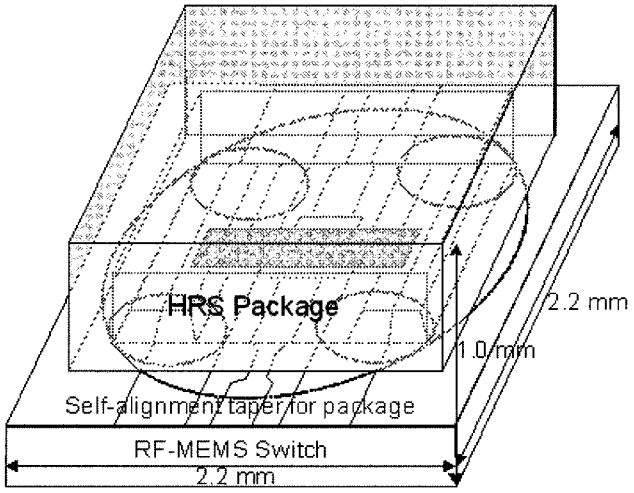

Fig. 10. Full package of RF-MEMS switch.

Fig. 11. Photograph of RF-MEMS switch with package.

0.31, respectively. The very low stress in corrugation region is shown by von mises stress in Fig. 12. The xy shear stresses of flat and corrugated bridges are 26.5 MPa and 21.9 MPa, respectively, as shown in Fig. 13.

4-2 RF-MEMS Switch with Package

The measurements are taken on a wafer probe station using: 1) HP 8510C Vector Network Analyzer; 2) CASCADE MICROTECH GSG150 coplanar probes; 3) SOLT(Short/Open/Load/Thru) calibration technique, in a frequency range of 0.5~40 GHz. The DC bias voltage

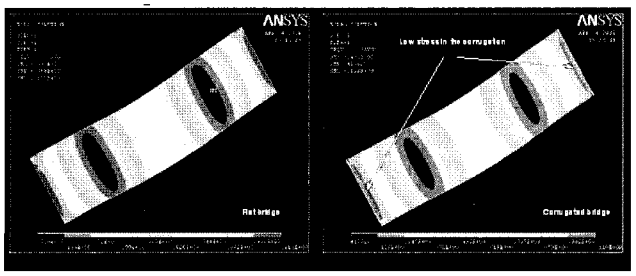

Fig. 12. Von mises stress of the flat and corrugated bridges.

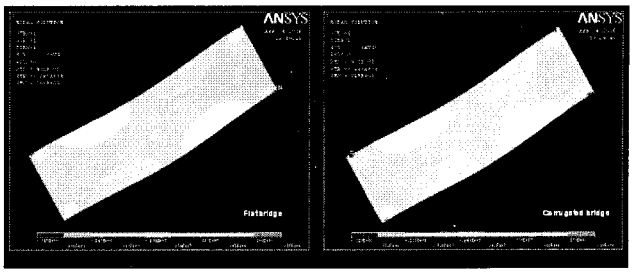

Fig. 13. XY shear stress of the flat and corrugated bridges.

is taken on between the signal and the ground of the CPW through two bias tees(Agilent 11612A) by a DC power supply.

The actuation voltages of the corrugated and flat switch are measured as various thickness bridges in Table 1. The residual stresses of the bridges are measured and calculated as shown in Tables 2, 3. The corrugated switches on concave structure require lower actuation voltages 20~80 V than 50~100 V of the flat switches on planar structure in 0.3 to 1.0 μm (0.1 μm step) thick Ni membranes for the RF-MEMS switch. The actuation voltage of corrugated switch on concave structure is lower than that of flat switch on planar structure. The effective residual stresses are measured and calculated about 3~15 MPa in the corrugated bridge on concave structure and 30 MPa in the flat bridge on planar struc-

Table 1. Measured actuation voltage.

Type \ Ni Thickness (μm)	0.3	0.4	0.5	0.6	0.7	0.8	0.9	1.0
Corrugated Switch(V)	20	25	30	40	50	60	70	80
Flat Switch(V)	50	55	60	70	80	85	95	100

Table 2. Calculated residual stress of the flat switch.

t (*um*)	V (V^p)	k'	k''	k	σ_0 (*MPa*)	Remark
1.0	100	13.06	33.63	46.69	30.46	
0.9	95	9.52	32.62	42.14	32.83	
0.8	85	6.69	27.05	33.73	30.62	
0.7	80	4.48	25.40	29.88	32.87	E: 200 *GPa*
0.6	70	2.82	20.06	22.88	30.28	v: 0.31
0.5	60	1.63	15.18	16.81	27.49	l: 300 *um*
0.4	55	0.84	13.29	14.12	30.09	g_0: 4 *um*
0.3	50	0.35	11.32	11.67	34.18	

Table 3. Calculated residual stress of the corrugated switch.

t (um)	V (V^p)	k'	k''	k	σ_{meas} (MPa)	σ_{Cal} (MPa)	E_{eff} (GPa)
1.0	80	13.06	16.82	29.88	15.24	15.91	3.70
0.9	70	9.52	13.36	22.88	13.44	15.41	3.00
0.8	60	6.69	10.12	16.81	11.46	12.60	2.37
0.7	50	4.48	7.19	11.67	9.31	11.46	1.81
0.6	40	2.82	4.65	7.47	7.02	8.55	1.33
0.5	30	1.63	2.57	4.20	4.65	5.90	0.93
0.4	25	0.84	2.08	2.92	4.72	4.48	0.59
0.3	20	0.35	1.51	1.87	4.57	3.06	0.33

ture as shown in Figs. 14, 15. The intrinsic residual stress is about 30 MPa in the flat bridge regardless of the various thickness membranes[35],[36].

Therefore, the corrugation ratios σ / σ_0 of the bridges with corrugated structure are 0.13~0.5 due to the various thickness membrane 0.3~1.0 μm by 0.1 μm step. The residual stress is very low in the corrugated bridge on concave structure because having both ends corrugated structure of the bridge. The effective residual stress in the bridge structure is critical to actuation voltage of the switch. The corrugated structure has also been observed to significantly alter the actuation voltage for this switch design.

The insertion loss, return loss, power loss, and isolation of the switch are shown in Figs. 16, 17. The insertion loss of the shunt switch in the up-state position is nearly equal to the loss of the transmission line and is around 1.0 dB up to 40 GHz. As expected, the return loss 12 dB is greater for the unmatched transmission line because of the package feed-through. Therefore, the power loss is 10 dB up to 40 GHz in Fig. 16. When the bridge is down, the signal is attenuated by isolation 29 dB and power loss 10 dB up to 40 GHz using a CPW line with a narrow gap in the SiO_2(ε_r=4) insulator

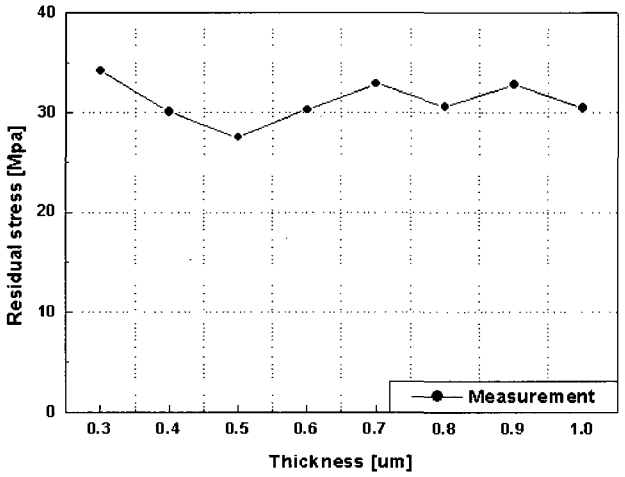

Fig. 14. Residual stress of the flat switch.

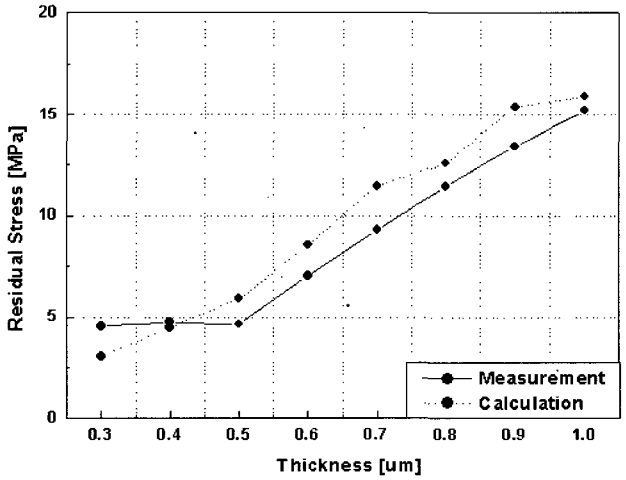

Fig. 15. Residual stress of the corrugated switch.

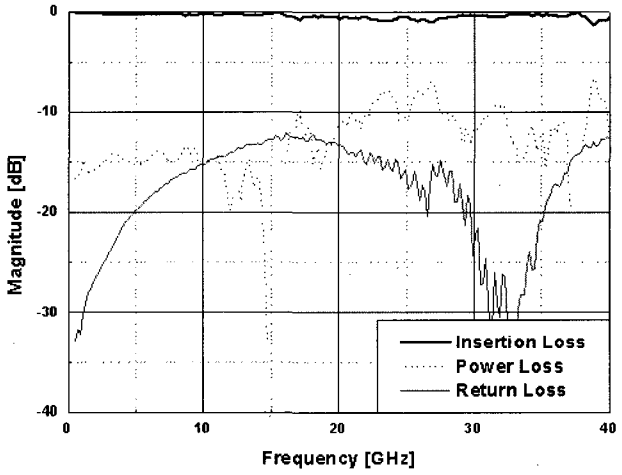

Fig. 16. Insertion, return, and power loss of the switch.

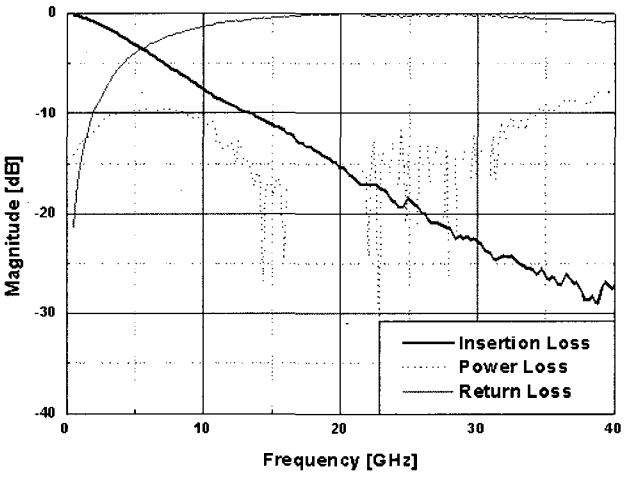

Fig. 17. Isolation, return, and power loss of the switch.

and a low inductance to ground is achieved in Fig. 17. As expect, the isolation of the Si_3N_4(ε_r=9) may be greater than that of the SiO_2(ε_r=4) insulator with frequency.

The RF-MEMS switch is packaged using a HRS MEMS package with a conductor-backed metal chip carrier in order to observe coplanar parasitic problems of leakage, coupling, and resonance. The packaged HRS MEMS package scheme is verified by fabricating and measuring the HRS MEMS package with the RF-MEMS switch on 15 Ω · cm lightly-doped Si chip carrier in the frequency range from 0.5 to 40 GHz. The S-parameters of the full RF-MEMS switch with the HRS MEMS package containing a 15 Ω · cm lightly-doped Si chip carrier are measured and compared each other in Figs. 18, 19. The fluctuations of the S-parameters are greatly suppressed as the lightly-doped Si layer absorbs the parasitic leakage resonances. The HRS MEMS package with a 15 Ω · cm lightly-doped Si chip carrier shows no parasitic leakage resonances in the whole frequency range. It is verified that the HRS MEMS package with a lightly-doped Si chip carrier can be an effective packaging solution for the low cost and high performance coplanar MMICs[35],[36].

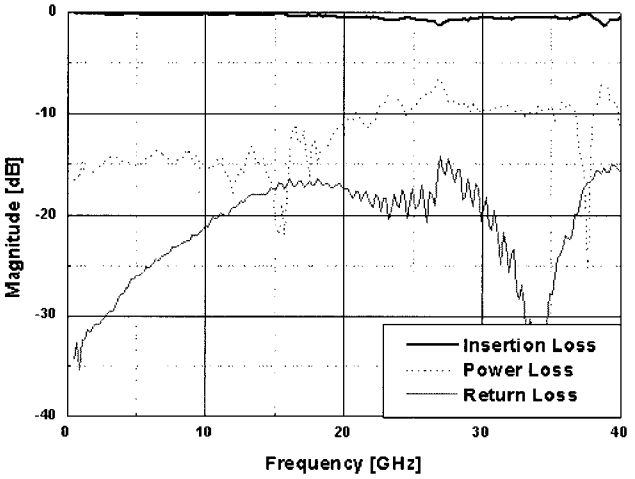

Fig. 18. Insertion, return, and power loss of the switch with package.

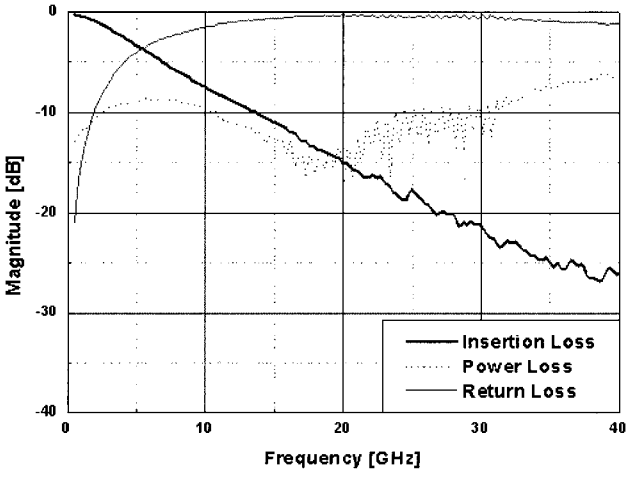

Fig. 19. Isolation, return, and power loss of the switch with package.

The insertion loss, the return loss, the power loss, and the isolation of the RF MEMS switch with the HRS MEMS package are, respectively, less than 1.0 dB, 15 dB, 10 dB, and 28 dB up to 40 GHz.

V. Conclusions

This paper has presented the experimental results on the low actuation voltage capacitive shunt RF-MEMS switch having a corrugated membrane with self-alignment HRS MEMS package for the low cost and high performance CPW MMICs applications.

The corrugated switches have been fabricated and measured using a simple mask design process and 0.3 ~ 1.0 μm (0.1 μm step) thick membranes made up of sputtered nickel. It has been verified that the actuation voltage of corrugated switch on concave structure is lower than that of flat switch on planar structure. The static deflection and the stress of the bridges have also been proved by the finite element method(FEM) calculation.

The actuation voltage of corrugated switch with concave structure is lower than that of flat switch with planar structure. The residual stress is low in the corrugated switch with concave structure because having both ends corrugated structure of the bridge. Corrugating a membrane at the both ends of the switch on concave structure effectively releases the residual stress in the membrane, and expects to achieve lower actuation voltage than the switch built on flat membrane on planar structure. The effective residual stress in the bridge structure is critical to actuation voltage of the switch. The corrugated structure has also been observed to significantly alter the actuation voltage for this switch design.

The Self-alignment HRS MEMS package of the RF-MEMS switch with a lightly-doped Si chip carrier has also shown no parasitic leakage resonances in the whole frequency range. It has been verified that the HRS MEMS package with a lightly-doped Si chip carrier can be an effective packaging solution for the low cost and high performance coplanar MMICs.

References

[1] J. J. Yao, "RF MEMS from a device perspective", *J. Micromech. Microeng.*, vol. 10, pp. R9-R38, 2000.

[2] C. L. Goldsmith, Z. Yao, S. Eshelman, and D. Denniston, "Performance of low-loss RF MEMS capacitive switches", *IEEE Microwave Guided Wave Lett.*, vol. 8, no. 8, pp. 269-271, Aug. 1998.

[3] C. Goldsmith, J. Randall, S. Eshelman, T. H. Lin, D. Denniston, S. Chen, and B. Norvell, "Characteristics of micromachined switches at microwave frequencies", *IEEE MTT-S Int. Microwave Symp. Dig.*, San Francisco, CA, pp. 1141-1144, Jun. 1996.

[4] J. J. Yao, M. F. Chang, "A surface micromachined miniature switch for telecommunications applications with signal frequencies from DC up to 4 GHz", *Int. Conf. Solid-State Sens. Actuators Dig.*, Stockholm, Sweden, pp. 384-387, Jun. 1995.

[5] G. M. Rebeiz, J. B. Muldavin, "RF MEMS switches and switch circuits", *IEEE Microwave Mag.*, vol. 2, pp. 59-71, Dec. 2001.

[6] E. R. Brown, "RF-MEMS switches for reconfigurable integrated circuits", *IEEE Trans. Microwave Theory Tech.*, vol. 46, pp. 1868-1880, Nov. 1998.

[7] K. E. Petersen, "Dynamic micromechanics on silicon: techniques and devices", *IEEE Trans. Electron Devices*, vol. 25, no. 10, pp. 1241-1250, Oct. 1978.

[8] L. E. Larson, R. H. Hackette, and R. F. Lohr, "Microactuators for GaAs-based microwave integrated circuits", *Transducers'91 Int. Conf. Solid-State Sens. Actuators Dig.*, San Francisco, CA, pp. 743-746, Jun. 1991.

[9] S. P. Pacheco, L. P. B. Katehi, and T. C. Nguyen, "Design of low actuation voltage RF MEMS switch", *IEEE MTT-S Int. Microwave Symp. Dig.*, pp. 165-168, 2000.

[10] Z. J. Yao, S. Chen, S. Eshelman, D. Denniston, and C. Goldsmith, "Micromachined low-loss microwave switches", *IEEE J. Microelectromech. Syst.*, vol. 8, no. 2, pp. 129-134, Jun. 1999.

[11] D. Peroulis, K. Sarabandi, and L. P. B. Katehi, "Low contact resistance series MEMS switches", *IEEE MTT-S Int. Microwave Symp. Dig.*, pp. 223-226, 2002.

[12] S. Duffy, C. Bozler, S. Rabe, J. Knecht, L. Travis, P. Wyatt, C. Keast, and M. Gouker, "MEMS microswitches for reconfigurable microwave circuitry", *IEEE Microwave Wireless Comp. Lett.*, vol. 11, pp. 106-108, Mar. 2001.

[13] J. B. Muldavin, G. M. Rebeiz, "High-isolation CPW MEMS shunt switches-part 1: modeling", *IEEE Trans. Microwave Theory and Techniques*, vol. 48, no. 6, pp. 1045-1052, Jun. 2000.

[14] D. Hyman, M. Mehregany, "Contact physics of gold microcontacts for MEMS switches", *IEEE Trans. Comp. Packag. Technol.*, vol. 22, no. 3, pp. 357-364, Sep. 1999.

[15] M. Kim, J. B. Hacker, R. E. Mihailovich, and J. F. DeNatale, "A DC-to-40 GHz four-bit RF-MEMS true-time delay network", *IEEE Microwave Wireless Comp. Lett.*, vol. 11, no. 2, pp. 56-58, Feb. 2001.

[16] J. Y. Park, G. H. Kim, K. W. Chung, and J. U. Bu, "Monolithically integrated micromachined RF MEMS capacitive switches", *Sens. Actuators A*, vol. 89, pp. 88-94. 2001.

[17] F. Plotz, S. Michaelis, R. Aigner, H. J. Timme, J. Binder, and R. Noe, "A low-voltage torsional actuator for application in RF-microswitches", *Sens. Actuators A*, vol. 92, pp. 312-317, 2001.

[18] J. M. Huang, K. M. Liew, C. H. Wong, S. Rajendran, M. J. Tan, and A. Q. Liu, "Mechanical design and optimization of capacitive micromachined switch", *Sens. Actuators A*, vol. 93, pp. 273-285, 2001.

[19] W. P. Taylor, M. G. Allen, "Integrated magnetic microrelays: normally open, normally closed, and multi-pole devices", *Transducers'97 Int. Conf. Solid-State Sens. Actuators Dig.*, Chicago, pp. 1149-1152, Jun. 1997.

[20] H. A. C. Tilmans, E. Fullin, H. Ziad, M. D. J. Van de peer, J. Kesters, E. V. Geffen, J. Bergqvist, M. Pantus, E. Beyne, K. Baert, and F. Naso, "A fully-packaged electromagnetic microrelay", *IEEE Micro Electro Mechanical Systems*, Orlando, Florida, Jan. 1999.

[21] X. Q. Sun, K. R. Farmer, and W. N. Carr, "A bistable microrelay based on two-segment multimorph cantilever actuators", *IEEE Micro Electro Mechanical Systems*, Heidelberg, Germany, Jan. 1998.

[22] L. E. Larson, R. H. Hackett, M. A. Melendes, and R. F. Lohr, "Micromachined microwave actuator (MIMAC) technology- a new tuning approach for microwave integrated circuits", *IEEE MTT-S Int. Microwave Symp. Dig.*, pp. 27-30, Jun. 1991.

[23] K. J. Rangra, F. Giacomozzi, B. Margesin, L. Lorenzelli, V. Mulloni, C. Collini, R. Marcelli, and G. Soncini, "Micromachined low actuation voltage RF MEMS capacitive switches, technology and characterization", *Int. Semiconductor Conf.*, 2004.

[24] S. A. Frang, E. A. Sani, "A low voltage capacitive micromachined microwave switch", *ICSE*, Penang, Malaysia, pp. 110-114, Dec. 2002.

[25] P. R. Scheeper, W. Olthuis, and P. Bergveld, "The design, fabrication, and testing of corrugated silicon nitride diaphragms", *J. Microelectromechanical*

Syst., vol. 3, no. 1, pp. 36-42, 1994.

[26] M. Fuldner, A. Dehe, and R. Lerch, "Analytical analysis and finite element simulation of advanced membranes for silicon microphones", *IEEE Sensors Journal*, vol. 5, no. 5, pp. 857-863, Oct. 2005.

[27] H. Yan, E. S. Kim, "Corrugated diaphragm for piezoelectric microphone", *IEEE EFTA*, pp. 503-506, 1996.

[28] M. Giovanni, *Flat and Corrugated Diaphragm Design Handbook*, Marcel Dekker Inc., New York, 1982.

[29] D. L. Logan, *Mechanics of Materials*, Harper Collins Publishers, New York, 1991.

[30] J. M. Gere, S. P. Timoshenko, *Mechanics of Materials*, 4th Edition, PWS Publishing Company, Boston, 1997.

[31] W. C. Young, R. G. Budynas, *Roark's Formulas for Stress and Strain*, 7th Edition, McGraw-Hill, New York, 2002.

[32] G. M. Rebeiz, *RF MEMS Theory, Design, and Technology*, John Wiley & Sons Inc., New Jersey, 2003.

[33] Y. T. Song, H. Y. Lee, and M. Esashi, "Resonance-free millimeter-wave coplanar waveguide Si microelectromechanical system package using a lightly-doped silicon chip carrier", *Japanese Journal of Applied Physics*, vol. 44, no. 4A, pp. 1693-1697, 2005.

[34] Y. T. Song, H. Y. Lee, and M. Esashi, "Parasitic leakage resonance-free HRS MEMS package for microwave and millimeter-wave", *Sensors and Actuators A*, vol. 126, pp. in press, 2006.

[35] Y. T. Song, H. Y. Lee, and M. Esashi, "Low actuation voltage capacitive shunt RF-MEMS switch having a corrugated bridge", *IEICE Trans. Electron.*, accepted, Jun. 2006.

[36] Y. T. Song, H. Y. Lee, and M. Esashi, "A corrugated bridge of low residual stress for RF-MEMS switch", *Sensors and Actuators A*, under review, Apr. 2006.

Yo-Tak Song

received the B.S. and M.S. degrees in electronics engineering from Ajou University, Suwon, Korea, in 1984 and 2001, respectively, and is currently working toward the Ph.D. degree in electronics engineering at Ajou University. His research interests include the areas of design, packaging, and characterization of RF-MEMS switch.

Hai-Young Lee

received the B.S. degree in electronics engineering from Ajou University, Suwon, Korea, in 1980, the M.S. degree in electrical engineering from the Korea Advanced Institute of Science and Technology, Seoul, Korea, in 1982, and the Ph.D. degree in electrical engineering from The University of Texas at Austin, in 1989. From 1982 to 1986, he was with the Ministry of National Defense, Seoul, Korea, as a Senior Research Engineer in the fields of electromagnetic compatibility and wave propagation. In 1998, he was a Visiting Professor at the University of California at Los Angeles. From 1990 to 1992, he was in charge of the Advanced Research Section at the LG Electronics Institute of Technology, Seoul, Korea, Since 1992, he has been with the Department of Electronics Engineering, Ajou University, Suwon, Korea, as a Professor. His current research interest lies in the fields of RFIC design and testing, system-in-a-package, and high-speed interconnections and EMI/EMC for digital applications.

Masayoshi Esashi

received the B.S. and Ph.D. degrees in Electronic Engineering from Tohoku University in 1971 and 1976, respectively. From 1976 to 1981, he served as a research associate at the Department of Electronic Engineering, Tohoku University and he served as an associate professor from 1981 to 1990. Since 1990, he has been a professor in the Department of Mechatronics and Precision Engineering, Tohoku University. He has been studying microsensors and microsystems fabricated by micromachining.